Applied Surface Science 258 (2011) 1261–1266

Contents lists available at SciVerse ScienceDirect

Applied Surface Science

journal homepage: www.elsevier.com/locate/apsusc

Effects of post-annealing on the structural and nanomechanical properties of Ga-doped ZnO thin films deposited on glass substrate by rf-magnetron sputtering

Szu-Ko Wang[a], Ting-Chun Lin[a], Sheng-Rui Jian[a,*], Jenh-Yih Juang[b], Jason S.-C. Jang[c], Jiun-Yi Tseng[d]

[a] Department of Materials Science and Engineering, I-Shou University, Kaohsiung 840, Taiwan
[b] Department of Electrophysics, National Chiao Tung University, Hsinchu 300, Taiwan
[c] Department of Mechanical Engineering, Institute of Materials Science & Engineering, National Central University, Chung-Li 320, Taiwan
[d] Institute of Physics, Academia Sinica, Taipei 11529, Taiwan

ARTICLE INFO

Article history:
Received 12 June 2011
Received in revised form 17 August 2011
Accepted 20 September 2011
Available online 24 September 2011

Keywords:
ZnO:Ga thin films
XRD
AFM
Nanoindentation
Hardness

ABSTRACT

In this study, the effects of post-annealing on the structure, surface morphology and nanomechanical properties of ZnO thin films doped with a nominal concentration of 3 at.% Ga (ZnO:Ga) are investigated using X-ray diffraction (XRD), atomic force microscopy (AFM) and scanning electron microscopy (SEM) and nanoindentation techniques. The ZnO:Ga thin films were deposited on the glass substrates at room temperature by radio frequency magnetron sputtering. Results revealed that the as-deposited ZnO:Ga thin films were polycrystalline albeit the low deposition temperature. Post-annealing carried out at 300, 400 and 500 °C, respectively, has resulted in progressive increase in both the average grain size and the surface roughness of the ZnO:Ga thin film, in addition to the improved thin films crystallinity. Moreover, the hardness and Young's modulus of ZnO:Ga thin films are measured by a Berkovich nanoindenter operated with the continuous contact stiffness measurements (CSM) option. The hardness and Young's modulus of ZnO:Ga thin films increased as the annealing temperature increased from 300 to 500 °C, with the best results being obtained at 500 °C.

© 2011 Elsevier B.V. All rights reserved.

1. Introduction

Transparent conductive oxides (TCOs) have become increasingly prominent in the fabrication of various devices such as heterojunction solar cells [1,2], gas sensors [3] and flat panel devices [4]. The efficiency and performance of these devices are largely dependent on the optical and electrical properties of the relevant TCO materials. Indium tin oxide (ITO) is the most widely used TCO due to its high transparency in the visible range (~90% at 550 nm), low resistivity ($\sim 2 \times 10^{-4}\ \Omega$ cm) and large work function (~4.8 eV) [5]. However, recently ITO has become prohibitively expensive, in addition to its lack of thermal stability. As a result, alternatives such as the impurity-doped ZnO have been actively investigated. Group III elements Al [6], Ga [7] and In [8] have been demonstrated to exhibit the characteristics of n-type dopants for ZnO. Among them, Ga is considered as one of the most promising dopants because the Ga–O covalent bond length (1.92 Å) is very close to that of the Zn–O (1.97 Å), which, in turn, is expected to result in the possibility of obtaining wide range of doping concentration with minimum extent of lattice deformation, even for high Ga doping concentration [9]. Furthermore, it has been shown that Ga is relatively oxidation resistive [10]. Previously, Ga-doped ZnO films have been obtained using a variety of deposition methods, namely sol–gel [11], chemical vapor deposition [12], molecular beam epitaxy [13], pulsed laser deposition [14] and radio-frequency magnetron sputtering (rf-sputtering) [15,16]. Among them, the rf-sputtering has been widely used for fabricating oxide thin films because of its advantages of high deposition rates, low cost, easy control and high efficiency for growing films with good quality.

In addition to monitoring the electric and optical properties through careful control of the processing parameters, successful fabrication of devices based on Ga-doped ZnO thin films requires better understanding of the mechanical characteristics of the films, since the contact loading during processing or packaging can significantly degrade the performance of these devices. Therefore, there is a growing demand of investigating the mechanical characteristics of materials, in particular in the nanoscale regime. Nowadays, nanoindentation is probably the most prominent technique used in nanomechanics to investigate and characterize the mechanical properties of the materials in the sub-micron scale. It has been widely used to study the elastic–plastic and fracture properties on the surfaces of bulk samples [17–19], thin films [20–23], as well as for small structures [24,25]. More recently, it became possible to perform controlled compression and shear tests on sub-micron nanostructures, such as nanopillars [26,27].

* Corresponding author. Tel.: +886 7 6577711x3130; fax: +886 7 6578444.
E-mail address: srjian@gmail.com (S.-R. Jian).

0169-4332/$ – see front matter © 2011 Elsevier B.V. All rights reserved.
doi:10.1016/j.apsusc.2011.09.088

This study is therefore focused on nanomechanical characterizations of Ga-doped ZnO thin films deposited at room-temperature on the glass substrates using rf-sputtering system at various annealing temperatures by means of nanoindentation technique. The structure and surface morphology of thin films were characterized using X-ray diffraction (XRD), atomic force microscopy (AFM) and scanning electron microscopy (SEM). Changes in mechanical properties for the ZnO:Ga thin films are discussed in conjunction with the variations in crystalline structure, grain size and surface morphology resulted from annealing.

2. Experimental details

The ZnO:Ga thin films investigated in the present study were deposited on Corning 1737F glass substrates at room temperature using rf-sputtering from a ZnO target with a nominal Ga-doping of 3 at.%. In this work, the thin films are ~500 nm thick. The detailed growth procedures can be found elsewhere [28]. The as-deposited films were subsequently post-annealed at the temperatures ranging from 300 °C to 500 °C for 1 h in atmosphere. The heating rate was set at 20 °C/s and it took about 30 min for the furnace to cool down to room temperature after annealing.

The crystal structure of ZnO:Ga thin films were analyzed by X-ray diffraction (Panalytical X'Pert XRD, Cu Kα, $\lambda = 1.5406$ Å). A scanning probe microscopy (SEM, Hitachi S-2700) is used to analyze the thin films cross-sectional structure and, the surface features are carried out using atomic force microscopy (AFM) (Topometrix-Accures-II). The surface roughness can be represented by center line average (R_a) and root-mean-square average (R_{RMS}) [29] in the following forms:

$$R_a = \frac{1}{n}\sum_{i=1}^{n}|z_i| \quad (1)$$

$$R_{RMS} = \sqrt{\frac{1}{n}\sum_{i=1}^{n}z_i^2} \quad (2)$$

The center line is the line that divides the profile in such a way such that the net deviation is zero. Both R_a and R_{RMS} measure the average vertical deviation of surface profile from the center line. It should be noted that these parameters can only be used to compare sample surfaces generated by the same method [30].

Nanoindentation was conducted at room temperature using the MTS NanoXP® system (MTS Corporation, Nano Instruments Innovation Center, Oak Ridge, TN, USA) with force and displacement resolutions of 50 nN and 0.1 nm, respectively. A Berkovich diamond indenter was pressed into the films up to 80 nm with a strain rate varying from 0.01 s^{-1} to 1 s^{-1} and additional harmonic movements were simultaneously performed with the amplitude and frequency being set at 2 nm and 45 Hz, respectively, following the continuous stiffness measurements (CSM) technique [31]. The indenter was then held at the peak load for 10 s before it was completely withdrawn from the specimen to avoid the influence of creep on unloading characteristics, which were used to compute mechanical properties of the specimen. Each of the tests was performed when the thermal drift dropped to less than 0.01 nm/s. At least 20 indents, each two separated by 10 μm to avoid mutual interaction, were conducted on each sample. It is generally accepted that the indentation depth should never exceed 30% of the films thickness to avoid the substrate effect on hardness and modulus measurements [24]. Our samples and tests methodology were considered to adequate based on this concept. We also followed the analytic method proposed by Oliver and Pharr [32] to determine the hardness and Young's modulus of as-deposited and the annealed ZnO:Ga thin films from the load–displacement results. In this work, hardness and Young's modulus are obtained as a continuous function of penetration depth.

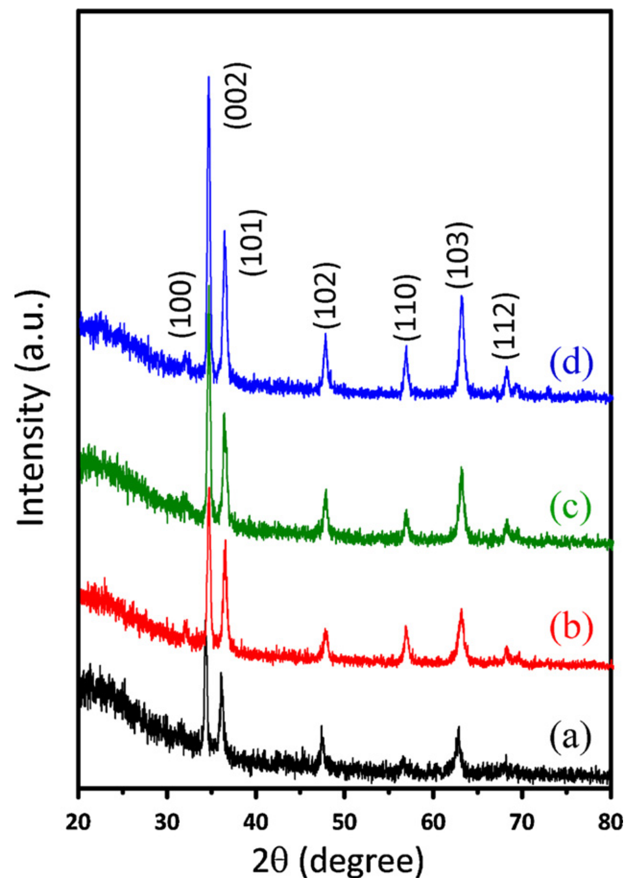

Fig. 1. XRD patterns of (a) as-deposited ZnO:Ga thin film, and annealed ZnO:Ga thin films at the different annealing temperatures of (b) 300 °C, (c) 400 °C and (d) 500 °C.

3. Results and discussion

The crystal structures and the level of crystallinity for all ZnO:Ga thin films were identified by XRD, as displayed in Fig. 1. The obtained XRD patterns correspond to the indexed six diffraction peaks of wurtzite structured crystalline ZnO (JCPDS 36-1451). It is evident that increasing the annealing temperature not only leads to significant increase in the intensity of major diffraction peaks, such as (0 0 2), (1 0 1), and (1 0 3) peaks, but also induces the evolvement of new diffraction peaks, such as (1 1 0) and (1 1 2), that are otherwise absent in the as-deposited ZnO:Ga thin films. This is indicative that annealing does have noticeable influences on the microstructure of the films, which tends to drive the films to become more equiaxial. Assuming a homogenous strain across the ZnO:Ga thin films, the average grain size can be estimated from the full-width at half-maximum (FWHM) of (0 0 2) peak using the following Sherrer's relation [33]:

$$D = \frac{0.9\lambda}{B\cos\theta} \quad (3)$$

Here λ, B and θ denote the X-ray wavelength, the FWHM of (0 0 2) peak, and the corresponding Bragg diffraction angle, respectively. The estimated mean grain sizes of the as-deposited thin films is 23.5 nm and that for films annealed at 300 °C, 400 °C and 500 °C are 42.2, 60.4 and 70.8 nm, respectively. It is interesting to compare the current results with that observed for ZnO films deposited using atomic layer deposition (ALD). In that, the as-deposited

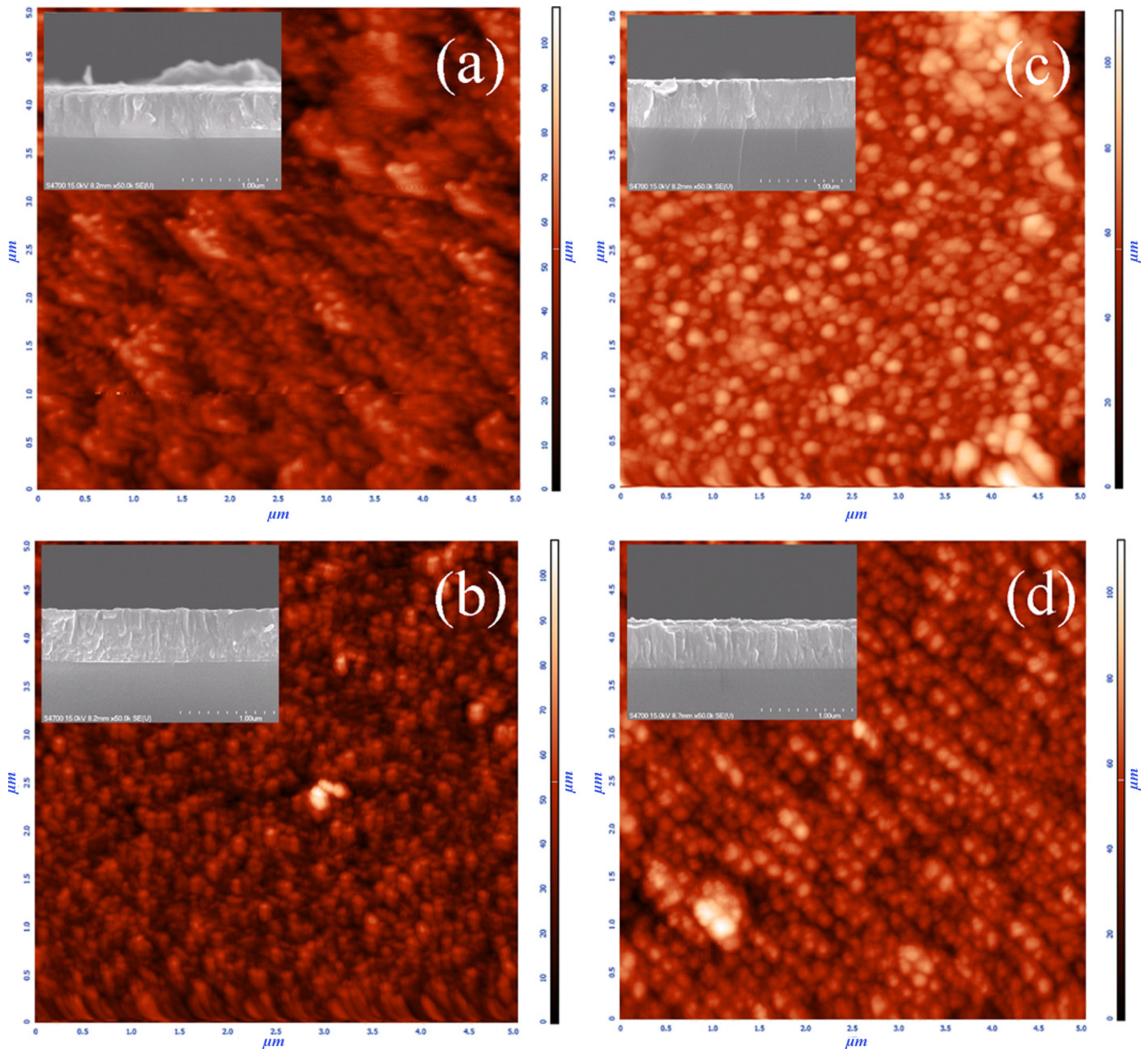

Fig. 2. AFM images of ZnO:Ga thin films: (a) as-deposited, and annealed at the different annealing temperatures of (b) 300 °C, (c) 400 °C and (d) 500 °C. The inset of each figure shows the corresponding cross-sectional SEM image.

ZnO thin films deposited at room-temperature appeared to be largely amorphous and subsequent annealing in the same temperature range resulted in smaller grain size, namely from 30 nm to 50 nm [34].

Fig. 2 displays the surface morphology of the corresponding ZnO:Ga thin films revealed by AFM. Although it is impossible to give a direct measure about the actual grain size from the AFM images, the results do exhibit apparent evolution in film grain morphologies with increasing annealing temperatures. The morphology starts with an appearance of patched grain clusters for the as-deposited film [Fig. 2(a)]. After subjected to 1 h annealing at 300 °C, it appears to evolve into individually distinctive grains [Fig. 2(b)]. Grain agglomerations are evident for films annealed at 400 °C [Fig. 2(c)]. For films annealed at 500 °C, grains evidently start to align along some specific orientations [Fig. 2(d)]. Since the films were grown on glass substrates and no epitaxial relation was expected, these phenomena might be understood as a direct consequence of surface diffusion enabled three-dimensional grain growth [34]. In this scenario, higher annealing temperatures lend more thermal energy to activate atom diffusion and, hence, facilitate the repairing the dislocated atomic occupancies and even promote the coalescence of adjacent grains [34,35]. As shown in the cross-sectional SEM images inserted in Fig. 2, the films are all with columnar structures. Thus, the major grain growth is expected to result in marked increase in both the effective grain size and the surface roughness of the resultant films [34–36]. Indeed, as shown in Fig. 3, the effective grain size estimated from the Sherrer's relation and the surface roughness obtained from the AFM measurements for all ZnO:Ga thin films do give rise to consistent results as expected.

The typical load–displacement curves for the as-deposited and the annealed ZnO:Ga thin films are displayed in Fig. 4.

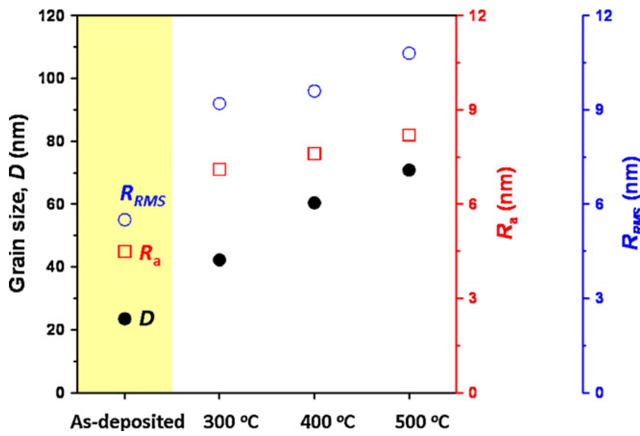

Fig. 3. Grain size (D), average surface roughness (R_a) and root-mean-square average surface roughness (R_{RMS}) of as-deposited and annealed ZnO:Ga thin films.

The load–displacement response obtained by nanoindentation contains information about the elastic and plastic deformation of the indented materials. Thus, it is often regarded as a "fingerprint" of the film properties under identification. Mechanical properties, such as the hardness and Young's modulus, can be readily extracted from the load–displacement curves like those displayed in Fig. 4. For instance, the hardness, H, being defined as the mean pressure under the indenter, can be calculated as the maximum applied load during indentation measurement, P_{max}, divided by the projection area, A_c, of contact between the indenter and the sample as expressed below,

$$H = \frac{P_{max}}{A_c} \tag{4}$$

The projection contact area is a function of the indenter's shape and the contact depth, h_c. For the case of an ideal pyramidal indenter, the area function (A_c) is given by [32]:

$$A_c \approx 24.5 h_c^2 \tag{5}$$

The contact depth prior to unloading thus can be directly estimated from the load–displacement data by the following expression [32]:

$$h_c = h_{max} - \varepsilon \frac{P_{max}}{S} \tag{6}$$

where ε is the geometric constant and, the value $\varepsilon = 0.72$ is generally used for a conical or pyramidal indenter [32], S is the experimentally measured stiffness of the upper portion of the unloading data, which is given by:

$$S = \frac{dP}{dh} \tag{7}$$

Similarly, Young's modulus is determined by assuming that the area in contact remains constant during initial unloading. The relationship between load and displacement on initial unloading is related to the stiffness of the sample and the indenter and, to the constant contact area between the sample and the indenter, and is given by [37]:

$$E_r = \frac{1}{2\beta} h_c \sqrt{\frac{\pi}{24.5}} \left(\frac{dP}{dh}\right) \tag{8}$$

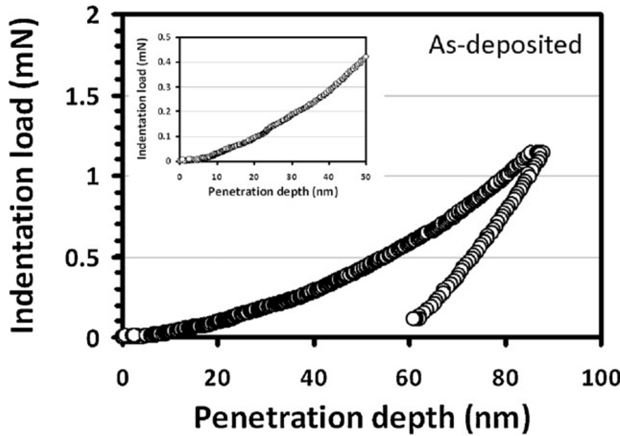

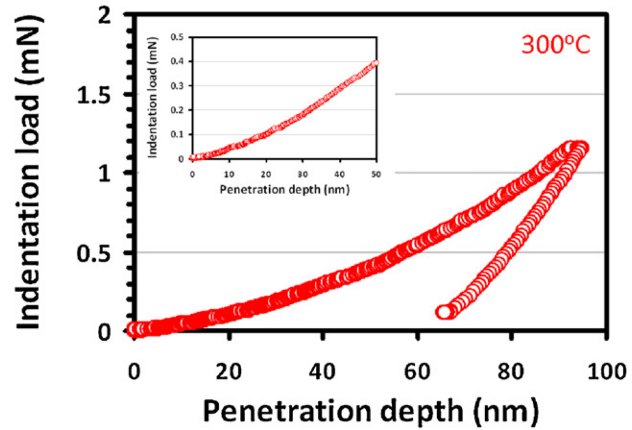

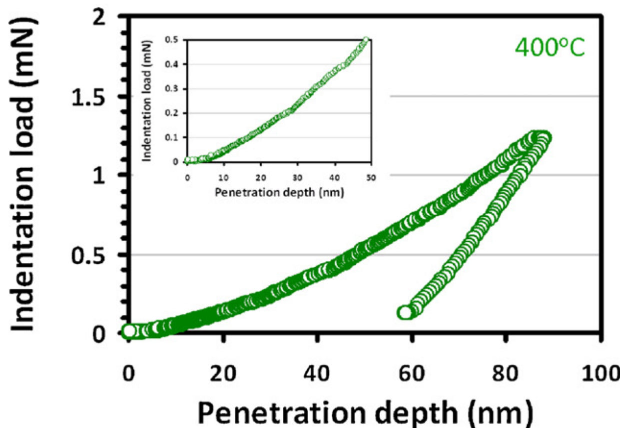

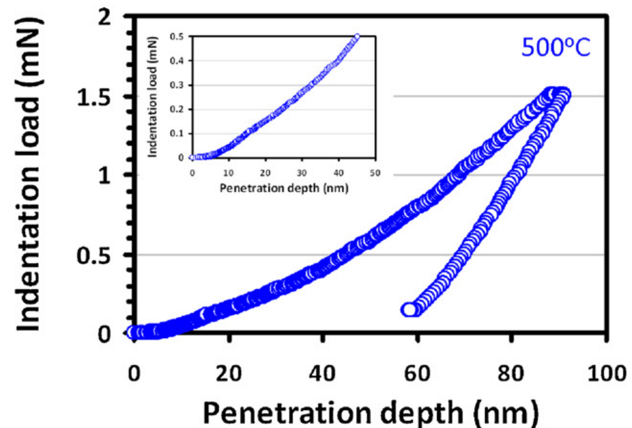

Fig. 4. The load–displacement curves of as-deposited and annealed ZnO:Ga thin films.

$$\frac{1}{E_r} = \frac{1-\nu^2}{E} + \frac{1-\nu_i^2}{E_i} \quad (9)$$

where β is a constant depending on the geometry of the indenter, E_r is the reduced modulus, E and ν are the Young's modulus and Poisson's ratio for the sample and, E_i and ν_i are the same parameters for the indenter. Poisson's ratio for the sample is assumed to be 0.25 [38] and, the elastic properties of the diamond indenter used in this study are E_i = 1141 GPa and ν_i = 0.07 [32].

The hardness and Young's modulus for the as-deposited and the annealed ZnO:Ga thin films as a function of penetration depth obtained using the analyses described above are illustrated in Fig. 5(a) and (b), respectively. As shown in Fig. 5(a), all of the hardness–displacement plots can be divided into two stages, namely, initial increase to a maximum value and subsequent decrease to a constant value. The increase in hardness at small penetration depth is usually attributed to the transition between purely elastic to elastic/plastic contact and at this stage the hardness is not accurately measured by the mean contact pressure. Only under the condition of a fully developed plastic zone does the mean contact pressure represent the hardness. When there is no plastic zone, or only partially formed plastic zone, the mean contact pressure is less than the nominal hardness [32]. After the first stage, the hardness decreases and reaches a constant value. The constant characteristic of hardness is consistent with that of a single material; therefore, the hardness values at this stage could be regarded as intrinsic properties of the films. The obtained hardness for the as-deposited ZnO:Ga thin films and those annealed at 300, 400 and 500 °C are 8.5, 7.4, 9.6, 11.8 GPa, respectively. The hardness values obtained from the abovementioned CSM measurements for all samples under study are summarized in Fig. 5. The initial drop of the hardness from 8.5 GPa to 7.4 GPa for the as-deposited ZnO:Ga thin film and that annealed at 300 °C is believed to result from the relaxation of residual stress in the film by the annealing process [39].

On the other hand, as displayed in Figs. 3 and 5, there is a clear tendency showing that, while increasing the annealing temperature has evidently increased the grain size of ZnO:Ga thin films, the annealing treatment has led to the increase of film hardness, as well. The results appeared to follow the notion of the inverse Hall–Petch effect [40]. It has been pointed out that dislocations are playing the primary role in the Hall–Petch effect, while for the inverse Hall–Petch effect grain boundary sliding is prominent for the film hardness [41,42]. Consequently, the behaviors observed here may be indicative that grain boundary structure is more relevant to the primary mechanical responses during indentation in the ZnO:Ga thin films. This might also explain the absence of apparent pop-in event in the load–displacement curves shown in Fig. 4, wherein the grain boundaries act the primary strain compensation sites and hence suppress the nucleation and propagation of threading dislocations needed for exhibiting pop-ins [43].

Fig. 5(b) displays a plot of Young's modulus of as-deposited and the annealed ZnO:Ga thin films determined using the method of Oliver and Pharr [32]. The tendency of variation is similar to the hardness results illustrated in Fig. 5(a). The values of Young's modulus for as-deposited film is 113.4 GPa, and that for films annealed at 300, 400, and 500 °C are 101.3, 120.6, 138.4 GPa, respectively (see Fig. 5(c)). Furthermore, the nanomechanical properties of ZnO thin films by nanoindentation are summarized in Table 1.

As discussed above, the nanoindentation-induced deformation in the present films behaves very differently from those expected for bulk ZnO [48]. Namely, the initiation of plastic deformation, instead of resulting from the sudden formation and rapid sliding of a large number of dislocations, may have been more relevant to grain boundary sliding and/or grain rotations [41,42]. Therefore, the generally larger grains (~40 to 70 nm) obtained in the current study as compared to that of the atomic-layer-deposition ZnO thin films, where grain size in the range of 30–50 nm were obtained [34], may explain the mechanical responses observed here. It is noted that doping might also modify the grain morphology and, hence, the mechanical behaviors of ZnO thin films. For instance, Zhao et al. [45] reported that boron doping can decrease the thickness of grain boundaries in pulsed laser deposited ZnO thin films, which eventually brought on improvement of films hardness.

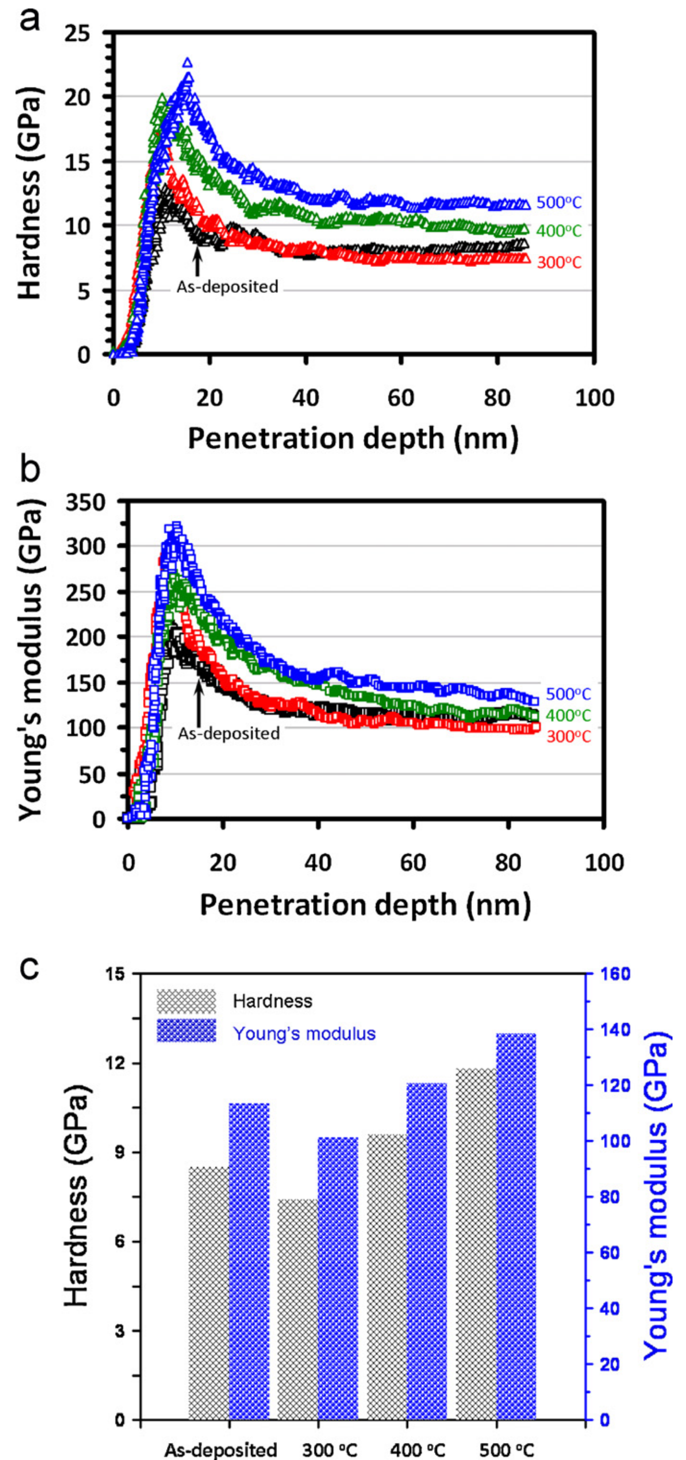

Fig. 5. Nanoindentation results: (a) the hardness and (b) Young's modulus vs. penetration depth curves of as-deposited and annealed ZnO:Ga thin films; (c) the hardness and Young's modulus of as-deposited and annealed ZnO:Ga thin films.

Table 1
The mechanical properties of ZnO thin films by nanoindentation.

ZnO films/a-SA	ZnO films/c-SA	ZnO films/6H-SiC	ZnO films	Al-doped ZnO films	Ga-doped ZnO films
H					
11.5 ± 0.8 GPa [38] 6.6 ± 1.2 GPa [44]	7.4 ± 0.1 GPa [38] 5.7 ± 0.8 GPa [44]	5.9 ± 0.2 GPa [38]	7.2–9.8 GPa [34] 9.3–12.1 GPa [45] 8.7 ± 0.2 GPa [46]	4.8 ± 1.3–7.1 ± 1.8 GPa [47]	7.4–11.8 GPa[a]
E					
212.2 ± 0.1 GPa [38] 318.2 ± 50 GPa [44]	150.1 ± 5.7 GPa [38] 310.1 ± 40 GPa [44]	117.1 ± 0.4 GPa [38]	139.5–168.6 GPa [34] 103.5–114.4 GPa [45] 154 ± 5 GPa [46]	87.9 ± 5.5–92.2 ± 12.6 GPa [47]	101.3–138.4 GPa[a]

SA: sapphire.
[a] The present study.

4. Conclusion

In conclusion, a combination of XRD, AFM, cross-sectional SEM and nanoindentation techniques has been carried out to investigate the microstructural and nanomechanical characteristics of ZnO:Ga thin films annealed at the various temperatures.

The XRD analysis showed that ZnO:Ga thin films were equi-axial polycrystalline in nature, albeit that predominant (0 0 2) orientation and a rougher surface morphology was gradually developed with increasing annealing temperature. Nanoindentation results indicated that, while the grain size was increased with increasing annealing temperature, the ZnO:Ga thin films have hardness ranging from 7.4 to 11.8 GPa and Young's modulus ranging from 101.3 to 138.4 GPa with increasing annealing temperature. The apparent inverse Hall–Petch effect is attributed to the grain boundary dominated mechanical responses as compared to the traditional dislocation threading mechanism.

Acknowledgements

This work was partially supported by the National Science Council of Taiwan, under Grant No.: NSC100-2221-E-214-024. J.Y.J. is partially supported by the MOE-ATU program operated at NCTU. Author likes to thank Dr. Y.-S. Lai, Dr. P.-F. Yang, Dr. G.-J. Chen and Dr. Y.-T. Chen for their technical supports.

References

[1] C. Lee, K. Lim, J. Song, Sol. Energy Mater. Sol. Cells 43 (1996) 37.
[2] C.G. Granqvist, Sol. Energy Mater. Sol. Cells 91 (2007) 1529.
[3] T. Kwon, S. Park, J. Ryu, H. Choi, Sens. Actuators B: Chem. 46 (1998) 75.
[4] D.S. Ginley, C. Bright, MRS Bull. 25 (2000) 15.
[5] H.L. Hartnagel, A.L. Dawar, A.K. Jain, C. Jagadish, Semiconductor Transparent Thin Films, Institute of Physics Publishing, Bristol and Philadelphia, 1995.
[6] J.J. Ding, H.X. Chen, S.Y. Ma, Appl. Surf. Sci. 256 (2010) 4304.
[7] X. Bie, J.G. Lu, L. Gong, L. Lin, B.H. Zhao, Z.Z. Ye, Appl. Surf. Sci. 256 (2009) 289.
[8] Y.R. Park, J. Kim, Y.S. Kim, Appl. Surf. Sci. 256 (2009) 1589.
[9] S.J. Henley, M.N.R. Ashfold, D. Cherns, Surf. Coat. Technol. 177 (2004) 271.
[10] V. Assunção, E. Fortunato, A. Marques, H. Águas, I. Ferreira, M.E.V. Costa, R. Martins, Thin Solid Films 427 (2003) 401.
[11] C.Y. Tsay, C.W. Wu, C.M. Lei, F.S. Chen, C.K. Lin, Thin Solid Films 519 (2010) 1516.
[12] A.R. Kaul, O.Y. Gorbenko, A.N. Botev, L.I. Burova, Superlattices Microstruct. 38 (2005) 272.
[13] H.J. Ko, Y.F. Chen, S.K. Hong, H. Wenisch, T. Yao, D.C. Look, Appl. Phys. Lett. 77 (2000) 3761.
[14] V. Bhosle, A. Tiwari, J. Narayan, J. Appl. Phys. 100 (2006) 033713.
[15] K. Yim, C. Lee, J. Mater. Sci. 18 (2007) 385.
[16] W.T. Yen, Y.C. Lin, P.C. Yao, J.H. Ke, Y.L. Chen, Thin Solid Films 518 (2010) 3882.
[17] P.F. Yang, Y.S. Lai, S.R. Jian, J. Chen, R.S. Chen, Mater. Sci. Eng. A 485 (2008) 305.
[18] S.R. Jian, J.B. Li, K.W. Chen, J.S.C. Jang, J.Y. Juang, P.J. Wei, J.F. Lin, Intermetallics 18 (2010) 1930.
[19] K.W. Chen, S.R. Jian, P.J. Wei, J.S.C. Jang, J.F. Lin, Intermetallics 18 (2010) 1572.
[20] J. Chen, S.J. Bull, J. Phys. D: Appl. Phys. 40 (2007) 5401.
[21] S.R. Jian, J.S.C. Jang, Y.S. Lai, P.F. Yang, C.S. Yang, H.C. Wen, C.H. Tsai, Mater. Chem. Phys. 109 (2008) 360.
[22] S.R. Jian, G.J. Chen, T.C. Lin, Nanoscale Res. Lett. 5 (2010) 935.
[23] S.R. Jian, J.Y. Juang, N.C. Chen, J.S.C. Jang, J.C. Huang, Y.S. Lai, Nanosci. Nanotechnol. Lett. 2 (2010) 315.
[24] X.D. Li, H.S. Gao, C.J. Murphy, K.K. Caswell, Nano Lett. 3 (2003) 1495.
[25] M.K. Kang, B. Li, P.S. Ho, R. Huang, J. Nanomater. 2008 (2008) 132728.
[26] Y.H. Lai, C.J. Lee, Y.T. Cheng, H.S. Chou, H.M. Chen, X.H. Du, C.I. Chang, J.C. Huang, S.R. Jian, J.S.C. Jang, T.G. Nieh, Scripta Mater. 58 (2008) 890.
[27] T.H. Sung, J.C. Huang, J.H. Hsu, S.R. Jian, Appl. Phys. Lett. 97 (2010) 171904.
[28] J.Y. Tseng, Y.T. Chen, M.Y. Yang, C.Y. Wang, P.C. Li, W.C. Yu, Y.F. Hsu, S.F. Wang, Thin Solid Films 517 (2009) 6310.
[29] K. Miyoshi, Y.W. Chung, Surface Diagnostics in Tribology: Fundamental Principles and Applications, World Scientific Publishing, Singapore, 1993.
[30] D. Cáceres, I. Vergara, R. González, E. Monroy, F. Calle, E. Muñoz, F. Omnès, J. Appl. Phys. 86 (1999) 6773.
[31] X.D. Li, B. Bhushan, Mater. Charact. 48 (2002) 11.
[32] W.C. Oliver, G.M. Pharr, J. Mater. Res. 7 (1992) 1564.
[33] B.D. Cullity, S.R. Stock, Element of X-Ray diffraction, Prentice Hall, New Jersey, 2001, p. 170.
[34] C.Y. Yen, S.R. Jian, G.J. Chen, C.M. Lin, H.Y. Lee, W.C. Ke, Y.Y. Liao, P.F. Yang, Y.S. Lai, J.S.C. Jang, J.Y. Juang, Appl. Surf. Sci. 257 (2011) 7900.
[35] Z.B. Fang, Z.J. Yan, Y.S. Tan, X.Q. Liu, Y.Y. Wang, Appl. Surf. Sci. 241 (2005) 303.
[36] X.Q. Wei, J.Z. Huang, M.Y. Zhang, Y. Du, B.Y. Man, Mater. Sci. Eng. B 166 (2010) 141.
[37] I.N. Sneddon, Int. J. Eng. Sci. 3 (1965) 47.
[38] S.R. Jian, I.J. Teng, P.F. Yang, Y.S. Lai, J.M. Lu, J.G. Chang, S.P. Ju, Nanoscale Res. Lett. 3 (2008) 186.
[39] H. Wang, S. Zhang, Y. Li, D. Sun, Thin Solid Films 516 (2008) 5419.
[40] J. Schiotz, T. Vegge, F.D. Di Tolla, K.W. Jacobsen, Phys. Rev. B 60 (1999) 11971.
[41] H. Van Swygenhoven, Science 296 (2002) 66.
[42] J. Chen, W. Wang, L.H. Qian, K. Lu, Scripta Mater. 49 (2003) 645.
[43] L.Y. Lin, D.E. Kim, Thin Solid Films 517 (2009) 1690.
[44] V.A. Coleman, J.E. Bradby, C. Jagadish, P. Munroe, Y.W. Heo, S.J. Pearton, D.P. Norton, M. Inoue, M. Yano, Appl. Phys. Lett. 86 (2005) 203105.
[45] S. Zhao, Y. Zhou, Y. Liu, K. Zhao, S. Wang, W. Xiang, Z. Liu, P. Han, Z. Zhang, Z. Chen, H. Lu, K. Jin, B. Cheng, G. Yang, Appl. Surf. Sci. 253 (2006) 726.
[46] R. Navamethavan, K.K. Kim, D.K. Hwang, S.J. Park, J.H. Hahn, T.G. Lee, G.S. Kim, Appl. Surf. Sci. 253 (2006) 464.
[47] L.Y. Lin, M.C. Jeong, D.E. Kim, J.M. Myoung, Surf. Coat. Technol. 201 (2006) 2547.
[48] S.R. Jian, J. Alloys Compd. 494 (2010) 214.